

# Numerical stress analysis for the multi-casing structure inside a wellbore in the formation using the boundary element method

Wan Cheng<sup>1,2</sup> · Yan Jin<sup>1</sup> · Mian Chen<sup>1</sup> · Guo-Sheng Jiang<sup>2</sup>

Received: 26 January 2016 / Published online: 22 December 2016  
© The Author(s) 2016. This article is published with open access at Springerlink.com

**Abstract** A multi-casing structure in drilling engineering can be considered as an inhomogeneous body consisting of many different materials. The mechanical behavior of the inhomogeneous body in an infinite domain is very complicated. In this paper, a detailed expression about the fictitious stress method of the boundary element method (BEM) is demonstrated for the inhomogeneous body. Then the fictitious stress method is deployed to investigate the stresses for the multi-casing structure under non-uniform loading conditions and an irregular wellbore. Three examples of the multi-casing structure in the borehole imply the high effectiveness of BEM for complex geometries related to the borehole in an infinite formation. The effects of casing eccentricity and the interfacial gap on the stress field are discussed. The eccentric casing takes the potential yield when the eccentric orientation is along the direction of  $S_h$ . Under different eccentric orientations, the von Mises stress in the casing increases with increasing degree of eccentricity. The radial stress in the multi-casing structure is always continuous along the radius, but the circumferential stress is discontinuous at the interface. The radial stress decreases and the circumferential stress increases with the increasing of the interfacial gap between the adjacent materials.

**Keywords** Displacement discontinuity method · Fictitious stress method · Drilling mechanics · Wellbore stress concentration · Inhomogeneous body

## 1 Introduction

Wellbore integrity investigation in drilling engineering involves stress and strength analyses of the pipe structure. The stresses in a thick-walled cylinder with open ends subjected to an internal pressure can be determined by Lamé's equation. The cross section of this cylinder belongs to a single-annulus structure (Fig. 1a). Similarly, the cross section of a metal pipe with an anti-corrosive coating (Luo et al. 2000) is usually treated as a double-annulus structure (Fig. 1b). The cross section of a lined circular tunnel at great depth (Bobet 2011) is usually treated as a single-annulus structure in an infinite plane (Fig. 1c). The cross section of a casing–cement sheath wellbore in the petroleum engineering is usually treated as a double-annulus structure in an infinite plane (Fig. 1d). Due to the symmetry of the loading condition and the geometry structure, the cross section of the problem in Fig. 1 satisfies the plane-strain condition.

Although analytical solutions for multi-annulus problems exist, such solutions are not available for problems where the annuluses are eccentric inside the wellbore or discontinuities exist. The boundary element method (BEM) will allow us to solve new and more realistic crack problems with complex geometry for geoscience applications (Ritz et al. 2012). BEM requires fewer boundary elements than the finite element method (FEM) when achieving the same accuracy (Ghassemi et al. 2001; Elleithy and Tanaka 2003; Ghassemi and Zhang 2004; Soares et al. 2004; Gun and Gao 2014; Cheng et al. 2015). The multi-annulus

✉ Wan Cheng  
chengwancup@163.com

<sup>1</sup> State Key Laboratory of Petroleum Resources and Prospecting, China University of Petroleum, Beijing 102249, China

<sup>2</sup> Faculty of Engineering, China University of Geosciences, Wuhan 430074, Hubei, China

Edited by Yan-Hua Sun

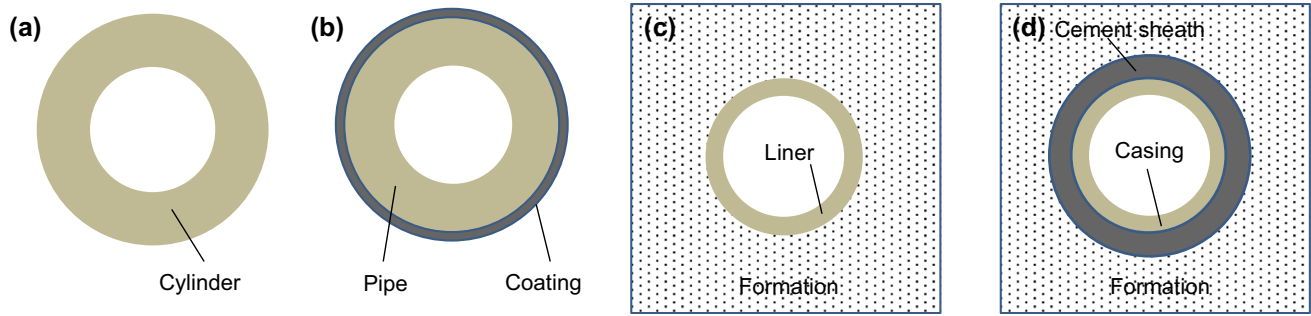


**Fig. 1** Cross section of engineering mechanical models. **a** Thick-walled cylinder. **b** Pipe with coating. **c** Lined circular tunnel. **d** Casing wellbore

structure consisting different materials belongs to a set of boundary value problems with the correlated constraints on the boundary conditions. Stress or displacement continuities for the interfaces of an inhomogeneous body (Zheng et al. 1991; Sladek et al. 1993; Park 2003; Kandilas 2012), as parts of constraints, are also required to solve the differential equations in the BEM. However, an interfacial crack (known as an interfacial gap) in an inhomogeneous body affects the contact behavior of two different materials under compression or tension, which probably leads to further unexpected failures (Crouch 1976; Crouch and Starfield 1983).

In this paper, the fictitious stress method in BEM is used for solving the stress in a multi-casing structure under non-uniform loading conditions and an irregular wellbore. The effects of the casing eccentricity and the interfacial gap on stress fields and strength are also discussed systematically. Several examples about the multi-casing structure in the borehole imply the high effectiveness of BEM for complex geometries in an infinite formation. We recommend a system with an infinite size, complex boundary geometry and boundary conditions and a low aspect ratio of mesh be solved by BEM.

## 2 BEM formulation for multi-annulus structures

### 2.1 Boundary element in an inhomogeneous body

An open wellbore in an infinite region is depicted in Fig. 2. The wall of the wellbore is labeled as  $\Gamma$  in a counterclockwise sense. The local coordinates  $n$  and  $s$  are, respectively, perpendicular and tangential to the boundary  $\Gamma$ ; they therefore vary from point to point along the boundary. We now imagine that constant resultant shear and normal stresses, which are applied on the boundary  $\Gamma$ , are denoted as fictitious stress (Ghassemi et al. 2001; Ghassemi and Zhang 2004)  $P_s$  and  $P_n$ , respectively. By contrast, the actual shear and normal stresses on curve  $\Gamma$  are, respectively, denoted as  $\sigma_s$  and  $\sigma_n$ ,

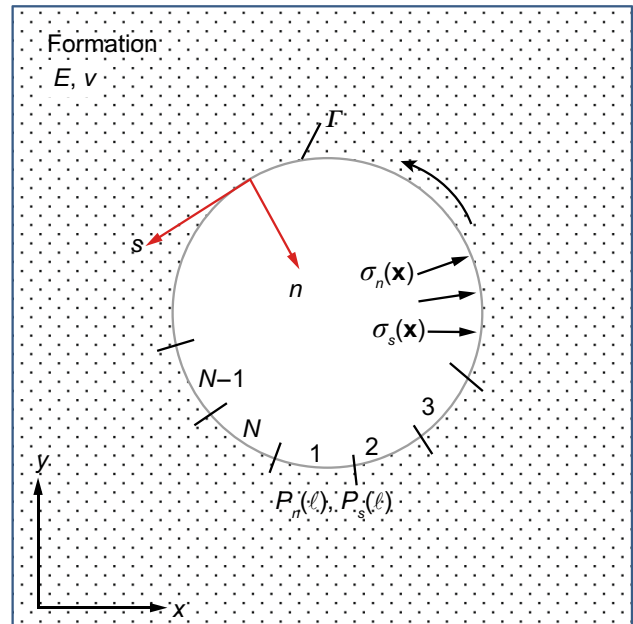


**Fig. 2** Section of an open wellbore

which are induced by  $P_s$  and  $P_n$ . In the absence of body force, the integral equations are given as follows

$$\sigma_i(\mathbf{x}) = \int_{\Gamma} G_{ij}(\mathbf{x}, \ell, E, \nu) P_j(\ell) d\ell \quad i = s, n; j = s, n \quad (1)$$

where  $\mathbf{x} = [x, y]$ ,  $\ell$  is the arc length of the boundary;  $G_{ij}$  represents the impact coefficient of the fictitious stress  $P_j$  under stress conditions;  $E$  and  $\nu$ , respectively, represent the elastic modulus and Poisson’s ratio of the material involved in the problem. Similarly, if displacements along the boundary are prescribed, the integral equations are given by

$$U_i(\mathbf{x}) = \int_{\Gamma} H_{ij}(\mathbf{x}, \ell, E, \nu) P_j(\ell) d\ell \quad i = s, n; j = s, n \quad (2)$$

where  $U_s$  and  $U_n$  represent the shear and normal displacements, respectively, and  $H_{ij}$  represents the impact coefficient of the fictitious stress  $P_j$  under displacement conditions.

Equation (1) is suitable for solving the engineering problem with stress boundary conditions, and Eq. (2) is suitable for the engineering problem with displacement boundary conditions. Mixed formulations involving the specification of stress and displacement boundary condition are handled by combining Eqs. (1) and (2). Since only one material represented by the elastic constant ( $E, \nu$ ) is involved in Eqs. (1) and (2), the integral equations are rewritten as

$$\begin{bmatrix} \boldsymbol{\sigma} \\ \mathbf{U} \end{bmatrix} = \int_{\Gamma} \begin{bmatrix} \mathbf{G} \\ \mathbf{H} \end{bmatrix} [\mathbf{P}] d\ell \tag{3}$$

where

$$\boldsymbol{\sigma} = \begin{bmatrix} \sigma_s \\ \sigma_n \end{bmatrix}, \mathbf{U} = \begin{bmatrix} U_s \\ U_n \end{bmatrix}, \mathbf{G} = \begin{bmatrix} G_{ss} & G_{sn} \\ G_{ns} & G_{nn} \end{bmatrix}, \tag{4}$$

$$\mathbf{H} = \begin{bmatrix} H_{ss} & H_{sn} \\ H_{ns} & H_{nn} \end{bmatrix}, \mathbf{P} = \begin{bmatrix} P_s(\ell) \\ P_n(\ell) \end{bmatrix}$$

A pipe in a linearly elastic body is depicted in Fig. 3. The inner and outer radius are labeled  $r_i$  and  $r_{i+1}$  ( $r_{i+1} > r_i$ ), respectively, while the inner and outer boundaries for the annulus region are represented by  $\Gamma(r_i^+)$  and  $\Gamma(r_{i+1}^-)$ , respectively. The inner boundary requires the boundary to be traversed in a counterclockwise sense, whereas the outer boundary requires a clockwise traversal, as shown in Fig. 3. Similar to Eq. (3), the integral equation of the single-annulus structure is given

$$\begin{bmatrix} \boldsymbol{\sigma} \\ \mathbf{U} \end{bmatrix} = \int_{\Gamma(r_i^+)+\Gamma(r_{i+1}^-)} \begin{bmatrix} \mathbf{G} \\ \mathbf{H} \end{bmatrix} [\mathbf{P}] d\ell \quad i = 1, 2, \dots, N - 1 \tag{5}$$

The cross section of the multi-annulus structure inside a long circular wellbore is depicted in Fig. 4. The radius of the circle is represented by  $r_i$  ( $i = 1, 2, 3, \dots, N$ ). The boundary of the formation is denoted as  $\Gamma(r_N^+)$ , while the

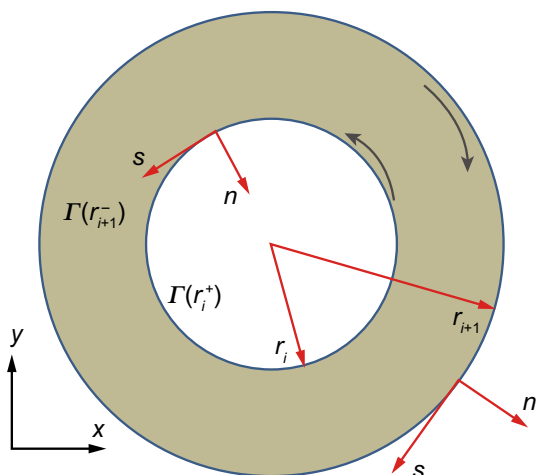


Fig. 3 Section of a long pipe

boundaries of the multi-annulus structure are denoted as  $\Gamma(r_i^+)$  and  $\Gamma(r_{i+1}^-)$  ( $i = 1, 2, 3, \dots, N - 1$ ).  $E_i$  and  $\nu_i$ , respectively, represent the elastic modulus and Poisson’s ratio of the material between  $\Gamma(r_i^+)$  and  $\Gamma(r_{i+1}^-)$ .  $E_N$  and  $\nu_N$  represent the elastic modulus and Poisson’s ratio of the formation, respectively. The general equations of BEM for the multi-annulus structure are expressed as follows:

$$\begin{bmatrix} \boldsymbol{\sigma}^{[i]} \\ \mathbf{U}^{[i]} \end{bmatrix} = \int_{\Gamma(r_i^+)+\Gamma(r_{i+1}^-)} \begin{bmatrix} \mathbf{G}^{[i]} \\ \mathbf{H}^{[i]} \end{bmatrix} [\mathbf{P}] d\ell \quad i = 1, 2, \dots, N - 1 \tag{6}$$

where the superscript  $i$  represents the  $i$ th material with the elastic constant ( $E_i, \nu_i$ ).

### 2.2 Boundary and contact conditions of multi-annulus systems

As shown in Fig. 4,  $P_0$  is the internal pressure acting inside the wellbore. The correlation between the global and local coordinates is given in Fig. 5.

The actual stresses on the boundary  $\Gamma(r_1^+)$  are given by

$$\begin{cases} \sigma_s|_{\Gamma(r_1^+)} = -\frac{1}{2}(\sigma_{yy} - \sigma_{xx}) \sin 2\beta + \sigma_{xy} \cos 2\beta \\ \sigma_n|_{\Gamma(r_1^+)} = P_0 - \sigma_{xx} \sin^2 \beta - \sigma_{yy} \cos^2 \beta + \sigma_{xy} \sin 2\beta \end{cases} \tag{7}$$

where  $\beta$  represents the angle between the local and global coordinate systems.

The interface between two isotropic, linearly elastic materials is depicted in Fig. 6. The interface can be treated as two separate problems, one for the material  $i$  and the other for material  $i + 1$ . The local coordinates  $n|_{\Gamma(r_i^-)}, s|_{\Gamma(r_i^-)}$  and  $n|_{\Gamma(r_i^+)}, s|_{\Gamma(r_i^+)}$  are oppositely directed along the interface,

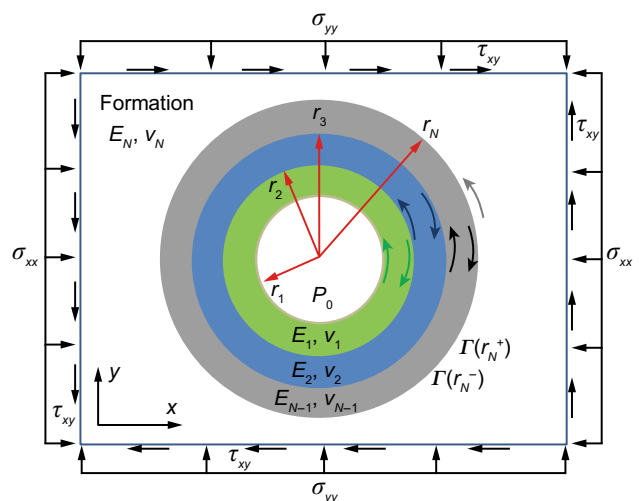


Fig. 4 Multi-annulus structure inside a long circular wellbore ( $\sigma_{xx}$ ,  $\sigma_{yy}$  and  $\sigma_{xy}$  represent the stress components)

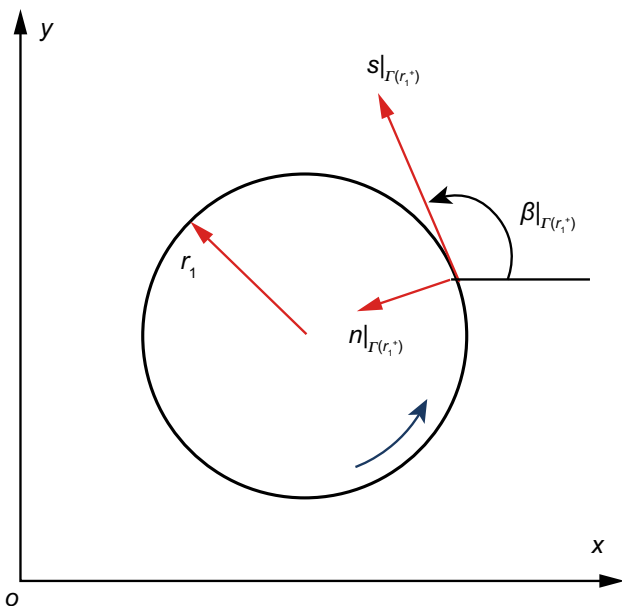


Fig. 5 Global and local coordinates

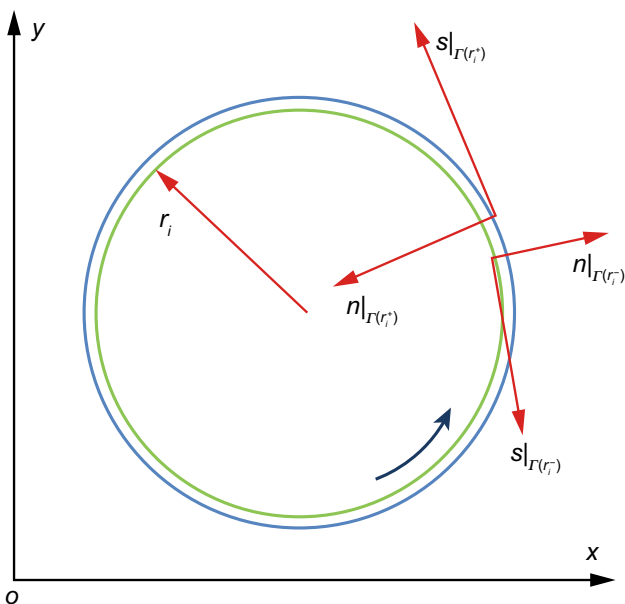


Fig. 6 Interface between two linearly elastic materials

$$n_{\Gamma(r_i^-)} = -n_{\Gamma(r_i^+)} \quad s_{\Gamma(r_i^-)} = -s_{\Gamma(r_i^+)} \quad i = 2, \dots, N \quad (8)$$

The continuity conditions for any point  $\mathbf{x}$  on the interface can be written as

$$\begin{cases} \sigma_s|_{\Gamma(r_i^-)} = \sigma_s|_{\Gamma(r_i^+)} & \sigma_n|_{\Gamma(r_i^-)} = \sigma_n|_{\Gamma(r_i^+)} \\ U_s|_{\Gamma(r_i^-)} = -U_s|_{\Gamma(r_i^+)} & U_n|_{\Gamma(r_i^-)} = -U_n|_{\Gamma(r_i^+)} \end{cases} \quad i = 2, \dots, N \quad (9)$$

The minus signs in Eq. (9) are a consequence of the opposite directions of the local coordinates  $n|_{\Gamma(r_i^-)}, s|_{\Gamma(r_i^-)}$

and  $n|_{\Gamma(r_i^+)}, s|_{\Gamma(r_i^+)}$  along the interface. Note that only the perfectly bonded parts of the interface satisfy the continuity conditions. The non-perfectly bonded parts, say an interfacial crack, will be considered as a displacement discontinuity.

$$U_s|_{\Gamma(r_i^-)} = \delta_s^{[i]} - U_s|_{\Gamma(r_i^+)} \quad U_n|_{\Gamma(r_i^-)} = \delta_n^{[i]} - U_n|_{\Gamma(r_i^+)} \quad (10)$$

$$i = 2, \dots, N$$

where  $\delta_s^{[i]}, \delta_n^{[i]}$ , respectively, represent the shear and normal displacements of the opened interface crack.

Note that if the outer radius of the  $i$ th annulus is smaller than the inner radius of the  $(i + 1)$ th annulus and this interfacial gap is initially larger than the deformation of the outer surface of the  $i$ th annulus, the  $(i + 1)$ th annulus will not suffer the expansion caused by the internal pressure inside the  $i$ th annulus, i.e., the annulus-wellbore structures should be separated as isolated problems from the interface between  $i$ th and  $(i + 1)$ th annulus. If the interfacial gap is initially smaller than the deformation of the outer surface of the  $i$ th annulus, the  $i$ th annulus must be expanded to fit the  $(i + 1)$ th annulus. By contrast, if the outer radius of the  $i$ th annulus is initially larger than the inner radius of the  $(i + 1)$ th annulus, the annulus must be compressed to fit them.

A line of symmetry exists for a certain problem when the elastic properties of the material, geometric configuration of the boundaries and the loading conditions are all symmetric with respect to the line in question. For a concentric annulus in a circular wellbore, such as in Fig. 4, a quarter of the structure can represent the full structure. If multiple eccentric annuli exist inside the wellbore, it requires all the boundaries to be divided into boundary elements. The use of symmetry conditions will involve fewer elements and less computation time.

### 2.3 Algebraic equations in the fictitious stress method

In setting up the algebraic equations in accordance with Eq. (6), it is convenient to divide the boundaries into  $m$  groups. The values of  $m$  are listed in Table 1 in accordance with Fig. 1.

Each group contains  $L_i$  ( $i = 1, 2, 3, \dots, m$ ) boundary elements. The total number of boundary elements is  $\sum_{i=1}^m L_i$ . It requires at least  $2 \sum_{i=1}^m L_i$  equations to solve all the fictitious stresses  $P_s$  and  $P_n$  on all the boundaries since each constant element contains both  $P_s$  and  $P_n$ .

As stated previously, an interface element actually consists of two coincident boundary elements. If the  $k$ th element is on the one side of interface, there will be a matching element  $k^*$ th on the other side. The matching

**Table 1** Number of groups in several critical models

Models	Figure 1a	Figure 1b	Figure 1c	Figure 1d	Figure 4
$m$	2	4	3	5	$2N - 1$

element satisfies the following condition when using Eq. (8).

$$\beta|_{\Gamma(r_i^+)} = \pi + \beta|_{\Gamma(r_i^-)} \quad i = 2, \dots, N \tag{11}$$

Equation (9) must be satisfied at each matching element. Therefore,

$$\begin{cases} \sigma_s^{[i]} - \sigma_s^{[i+1]} = 0 & \sigma_n^{[i]} - \sigma_n^{[i+1]} = 0 \\ U_s^{[i]} + U_s^{[i+1]} = 0 & U_n^{[i]} + U_n^{[i+1]} = 0 \end{cases} \tag{12}$$

Algebraic equations are given in Table 2. The first column indicates the boundaries of the multi-annulus structure, whereas the last column represents the boundary conditions. The central area (blue area) in Table 2 represents the coefficient matrix of the fictitious stresses. Proceeding in accordance with Table 2, we obtain a system of  $2 \sum_{i=1}^m L_i$  algebraic equations in  $2 \sum_{i=1}^m L_i$  unknown fictitious stress components. If an interfacial crack exists, [0] in the last column must be replaced by  $[\delta_s^{[i]} \delta_n^{[i]}]^T$ .

### 3 Verification of the BEM model

#### 3.1 Stress around an open hole

A fluid pressure is applied in the open wellbore of the impermeable and isotropic, linearly elastic formation, as shown in Fig. 2. The cross section of the wellbore is under far-field stresses  $S_H$  and  $S_h$ . An analytical solution (e.g., Wang et al. 2007) is available for this problem and reads

$$\begin{cases} S_{rr} = -P_0 \rho^2 + \frac{1}{2}(S_H + S_h)(1 - \rho^2) + \frac{1}{2}(S_H - S_h)(1 - 4\rho^2 + 3\rho^4) \cos 2\theta \\ S_{\theta\theta} = P_0 \rho^2 + \frac{1}{2}(S_H + S_h)(1 + \rho^2) - \frac{1}{2}(S_H - S_h)(1 + 3\rho^4) \cos 2\theta \end{cases} \quad \rho = R/r \tag{13}$$

where  $S_H, S_h$  represent the maximum and minimum in situ stresses in the far field, respectively;  $S_{rr}$  is the radial stress, MPa;  $S_{\theta\theta}$  is the circumferential stress (tangential stress), MPa;  $\theta$  is the azimuth measured counterclockwise from the direction of  $S_H$ , rad;  $P_0$  is the fluid pressure inside the wellbore, MPa;  $r$  is the inner radius of the wellbore while  $R$  is the distance from the circle center to the point in the

formation, m. Comparisons of the numerical and exact solutions are given in Fig. 7. Note that the “+” stands for the tensile stress while “-” stands for the compressive stress in this article. Only 80 elements are used in the BEM model, which saves the computational time but still achieves a high accuracy.

#### 3.2 Stress around a lined circular tunnel

As shown in Fig. 1c, the region of interest consists of a liner of  $a \leq r \leq b$  with elastic constants  $E_1$  and  $\nu_1$  inside a circular borehole of radius  $r = b$  with elastic constants  $E_2$  and  $\nu_2$  in an infinite formation. The internal wall of the annulus is subjected to the uniform pressure  $P_0$ , and the plate is unstressed at infinity. The analytical solution (e.g., Crouch and Starfield 1983) of this problem is

$$\begin{cases} S_{rr} = \frac{[P_0 a^2(1/b^2 - 1/R^2) + P'(a^2/R^2 - 1)]}{1 - a^2/b^2} \\ S_{\theta\theta} = \frac{[P_0 a^2(1/b^2 + 1/R^2) - P'(a^2/R^2 + 1)]}{1 - a^2/b^2} \end{cases} \quad a \leq R \leq b \tag{14}$$

$$S_{rr} = -P' \frac{b^2}{r^2}, S_{\theta\theta} = P' \frac{b^2}{r^2} \quad b \leq R \tag{15}$$

$$P' = \frac{2(1 - \nu_1)P_0 a^2 / b^2}{2(1 - \nu_1) + (1 - a^2/b^2) \left[ \frac{E_1(1 + \nu_2)}{E_2(1 + \nu_1)} - 1 \right]} \tag{16}$$

where  $a$  and  $b$  are the inner and outer radius of the annulus, respectively. The comparisons (Fig. 8) between the numerical and exact values prove the high accuracy of BEM. There exists a discontinuity of the circumferential stress at the annulus-formation interface, as shown in Fig. 8. The circumferential strain at the two sides of the interface is the same when the gap is zero. However, the circumferential strain will lead to different circumferential stresses (Fig. 8) due to two different material properties

around the interface. In other words, if Young’s modulus and Poisson’s ratio of the liner are the same as the formation, i.e.,  $E_1 = E_2, \nu_1 = \nu_2$ , the discontinuity of the circumferential stress will disappear. When  $E_1 = E_2, \nu_1 = \nu_2$  and the gap is zero, only one continuous medium is included in the model. The model is simplified as a pressurized wellbore inside an infinite, elastic medium.

**Table 2** Algebraic equations of multi-annulus structure in the wellbore

Boundary	Row $k$	Column $j$						Boundary value	
		$1 \leq j \leq \sum_{i=1}^2 L_i$	$\sum_{i=1}^2 L_i + 1 \leq j \leq \sum_{i=1}^4 L_i$	$\sum_{i=1}^4 L_i + 1 \leq j \leq \sum_{i=1}^6 L_i$	$\sum_{i=1}^6 L_i + 1 \leq j \leq \sum_{i=1}^8 L_i$	$\sum_{i=1}^{2(N-2)} L_i + 1 \leq j \leq \sum_{i=1}^{2(N-1)} L_i$	$\sum_{i=1}^{2(N-1)} L_i + 1 \leq j \leq \sum_{i=1}^{2N-1} L_i$		
$\Gamma(r_1^+)$	$1 \leq k \leq L_1$	$\mathbf{G}^{[1]}$	[0]	[0]	[0]	...	[0]	[0]	$[\boldsymbol{\sigma}]_{\Gamma(r_1^+)}$
$\Gamma(r_2^-)$	$L_1 + 1 \leq k \leq \sum_{i=1}^2 L_i$	$\mathbf{G}^{[1]}$	$-\mathbf{G}^{[2]}$	[0]	[0]	...	[0]	[0]	[0]
$\Gamma(r_2^+)$	$\sum_{i=1}^2 L_i + 1 \leq k \leq \sum_{i=1}^3 L_i$	$\mathbf{H}^{[1]}$	$\mathbf{H}^{[2]}$	[0]	[0]	...	[0]	[0]	[0]
$\Gamma(r_3^-)$	$\sum_{i=1}^3 L_i + 1 \leq k \leq \sum_{i=1}^4 L_i$	[0]	$\mathbf{G}^{[2]}$	$-\mathbf{G}^{[3]}$	[0]	...	[0]	[0]	[0]
$\Gamma(r_3^+)$	$\sum_{i=1}^4 L_i + 1 \leq k \leq \sum_{i=1}^5 L_i$	[0]	$\mathbf{H}^{[2]}$	$\mathbf{H}^{[3]}$	[0]	...	[0]	[0]	[0]
$\Gamma(r_4^-)$	$\sum_{i=1}^5 L_i + 1 \leq k \leq \sum_{i=1}^6 L_i$	[0]	[0]	$\mathbf{G}^{[3]}$	$-\mathbf{G}^{[4]}$	...	[0]	[0]	[0]
$\Gamma(r_4^+)$	$\sum_{i=1}^6 L_i + 1 \leq k \leq \sum_{i=1}^7 L_i$	[0]	[0]	$\mathbf{H}^{[3]}$	$\mathbf{H}^{[4]}$	...	[0]	[0]	[0]
...	...	...	...	...	...	...	...	...	...
$\Gamma(r_N^-)$	$\sum_{i=1}^{2N-3} L_i + 1 \leq k \leq \sum_{i=1}^{2N-2} L_i$	[0]	[0]	[0]	[0]	...	$\mathbf{G}^{[N-1]}$	$-\mathbf{G}^{[N]}$	[0]
$\Gamma(r_N^+)$	$\sum_{i=1}^{2N-2} L_i + 1 \leq k \leq \sum_{i=1}^{2N-1} L_i$	[0]	[0]	[0]	[0]	...	$\mathbf{H}^{[N-1]}$	$\mathbf{H}^{[N]}$	[0]

Another actual problem related to a lined circular tunnel is that the displacement continuity condition on the interface is not always perfect. An interfacial gap, say an opened interface crack, will be considered as a displacement discontinuity in Eq. (10). The numerical procedure in this paper still works very well. The radial stress is always continuous along the radius because of the stress equilibrium equation in the radial direction. By contrast, the circumferential stress is discontinuous at the interface because of the sudden change in the material properties at the interface (Fig. 9). The circumferential stress in the liner increases as the interfacial gap increases, but the circumferential stress in the formation decreases as the interfacial gap increases (Fig. 9). As mentioned in Sect. 2.2, when the interfacial gap is initially smaller than the deformation of the outer surface of the liner, the liner must be expanded to fit the inner surface of the formation. Then the pressure  $P_0$  will be transferred to the formation. When the interfacial gap is relative large, the liner will suffer a higher circumferential stress for expansion.

### 4 Engineering examples

#### 4.1 Example 1: stresses around an eccentric casing in the wellbore

The circle centers of wellbore and casing are denoted by  $o$  and  $o'$ , respectively. The inner radius of the wellbore is

represented by  $r_3$ , and the outer radius of the casing is represented by  $r_2$ . The eccentric degree of the casing is given by  $\Omega = |oo'|/(r_3 - r_2)$ , ( $\Omega \in [0, 1]$ ), as shown in Fig. 10. The eccentric orientation of the casing is given by  $\varphi$  ( $\varphi \in [0^\circ, 360^\circ]$ ). If  $\Omega = 0$ , the structure is symmetric in both the axes  $x$  and  $y$ . If  $\Omega \neq 0$ , the structure is still symmetric along the line  $oo'$ .  $[\Omega, \varphi]$  represents the state of the eccentric casing.

An actual case in a salt formation in the Tarim Basin, China, is given in Table 3. The elastic stress distribution inside the cement sheath is given in Fig. 11. Since it is difficult to observe the stress distribution inside the thin-walled casing, the annulus is extended as a rectangle in accordance with the radius and azimuth angle (Fig. 12).

The radial and circumferential stresses of the salt formation are given in Fig. 13. In the region far from the borehole center and along the axis  $x$ , the radial stress goes to  $S_H$  while the circumferential stress goes to  $S_h$ . In the region far from the borehole center and along the axis  $y$ , the radial stress goes to  $S_h$  while the circumferential stress goes to  $S_H$ . This implies the stress concentration disappears in the remote region.

The von Mises stress in the casing under different eccentricities is shown in Fig. 14. For the symmetry of geometry, the eccentric orientation from  $0^\circ$  to  $180^\circ$  is given in Fig. 14. Under the same eccentric degree, the von Mises stress increases with the eccentric orientation from  $0^\circ$  to  $90^\circ$  and decreases with the eccentric orientation from  $90^\circ$

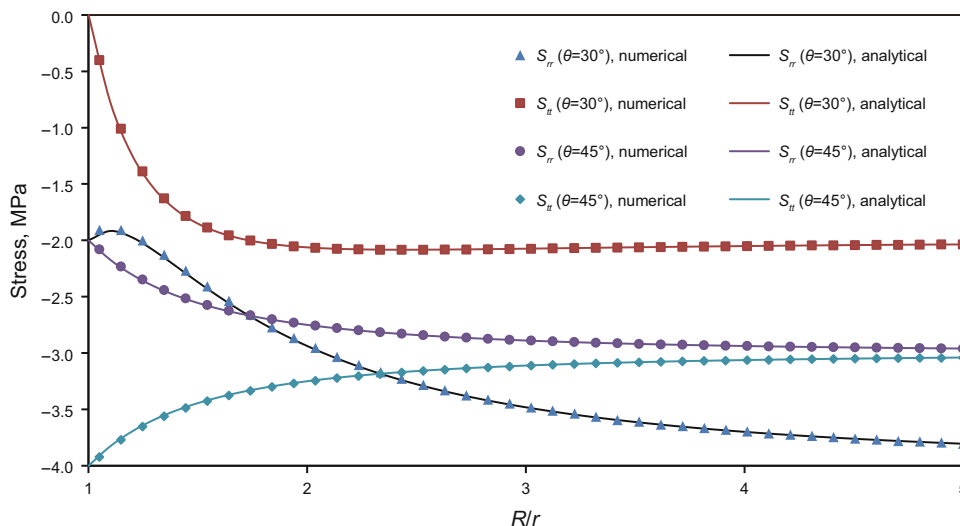


Fig. 7 Comparisons between analytical and numerical solutions ( $S_H = -5$  MPa;  $S_h = -1$  MPa;  $P_0 = 2$  MPa; 80 boundary elements in total)

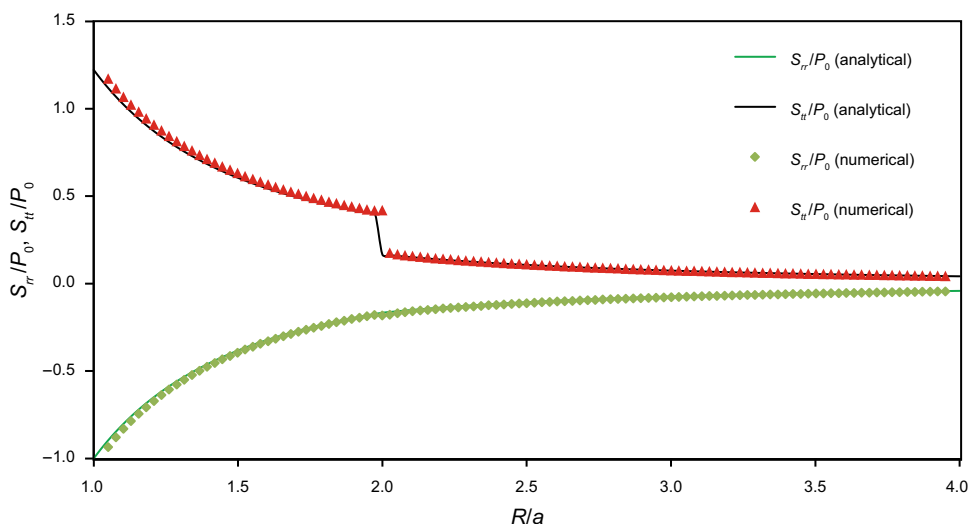


Fig. 8 Comparisons between analytical and numerical solutions ( $\nu_1 = 0.25$ ;  $E_1 = 50$  GPa;  $\nu_2 = 0.25$ ;  $E_2 = 25$  GPa;  $b = 2a$ ;  $S_H = \sigma_{xx} = 0$ ;  $S_h = \sigma_{yy} = 0$ ; 240 boundary elements in total)

to  $180^\circ$ . The von Mises stress reaches a maximum value at an eccentric orientation of  $90^\circ$ , i.e., the eccentric casing takes the potential yield when the eccentric orientation is along the direction of the minimum in situ stress  $S_h$ . Under different eccentric orientations, the von Mises stress increases with increasing eccentric degree. However, the von Mises stress changes little at different eccentric degrees, when  $\varphi = 0^\circ$  (the direction of  $S_H$ ).

#### 4.2 Example 2: stresses inside the multi-casing structure in the wellbore

Another actual case with two casings and two cement sheaths in a salt formation is given in Table 4. The cross

section of this case belongs to a multi-annulus structure. The inhomogeneity of the multi-casing structure from the center to the formation is denoted as casing–cement–casing–cement formation. For convenience, we assume that all the casings in the problem are concentric.

Since it is also difficult to observe the stress distribution inside the thin-walled annulus of the casing or the cement sheath, the annuli are extended as a rectangle in accordance with radius and azimuth angle, as shown in Fig. 15. The radial stress decreases with the radial distance from the borehole center. The radial stress is always continuous at the interface between the annuli, while the circumferential stress is continuous except the interface.

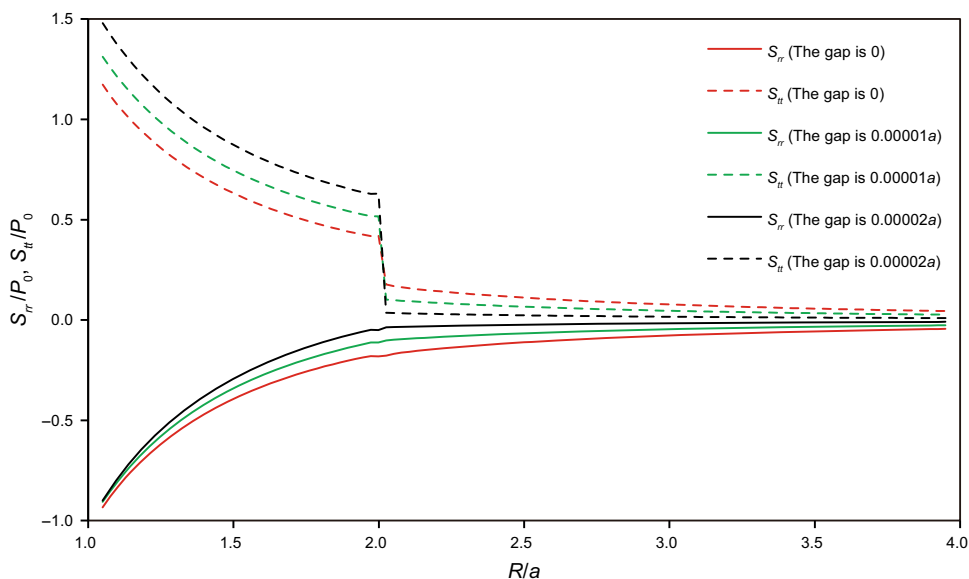


**Fig. 9** Stresses at different interfacial gaps ( $\nu_1 = 0.25$ ;  $E_1 = 50$  GPa;  $\nu_2 = 0.25$ ;  $E_2 = 25$  GPa;  $b = 2a$ ;  $S_H = \sigma_{xx} = 0$ ;  $S_h = \sigma_{yy} = 0$ ;  $P_0 = 1$  MPa; 240 boundary elements in total)

### 4.3 Example 3: stresses for a multi-annulus structure inside an irregular wellbore

After the breakout of the borehole, the new boundary of the borehole is obtained. The borehole is irregular after the breakouts during the process of drilling engineering (Mastin 1988; Zoback et al. 2003; Zhang et al. 2008). A casing is cemented inside the irregular wellbore in order to

keep the wellbore stable. This physical model is more similar to the actual situation in drilling engineering. Since the theoretical solution to this model does not exist in linearly elastic mechanics, the BEM is deployed to solve this model numerically. The basic parameters are listed in Table 5. The frictional coefficient and cohesion of the rock matrix are 0.5 and 5 MPa, respectively. The stress distribution in the cement sheath is given in Fig. 16, which helps the engineers to design the cement mud.

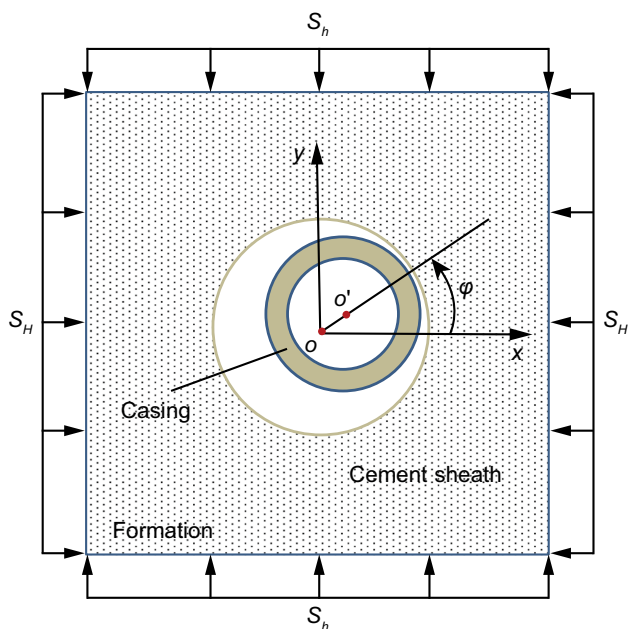


**Fig. 10** Eccentric casing in the wellbore (the azimuth angle is measured counterclockwise from  $S_H$ )

## 5 Conclusions

The application of the BEM on an inhomogeneous body consisting of many different materials offers many possibilities to solve complicated engineering problems with an irregular or regular geometry. A multi-casing structure in a wellbore in the formation belongs to a specific case of an inhomogeneous body. Three examples about a multi-casing structure in the borehole imply the high effectiveness of BEM for complex geometries in an infinite formation. A system with infinite size, complex boundary geometry and boundary conditions and low aspect ratio of mesh is highly recommended to be tackled by the BEM.

An eccentric casing takes the potential yield when the eccentric orientation is along the direction of  $S_h$ . Under different eccentric orientations, the von Mises stress in the casing increases with an increase in eccentric degree. It changes little at different eccentric degrees, when the eccentric orientation is along the direction of  $S_H$ . The radial stress in the multi-casing structure is always continuous

**Table 3** Related parameters of the wellbore in the Tarim Basin, China

$E_1, E_2, E_3$ , GPa	$\nu_1, \nu_2, \nu_3$	$r_1, r_2, r_3$ , mm	$S_H, S_h$ , MPa	$P_0$ , MPa	Eccentricity
210, 7, 5	0.30, 0.18, 0.45	109.5, 125.4, 155.6	-140, -134	61.25	[0.4, 60°]

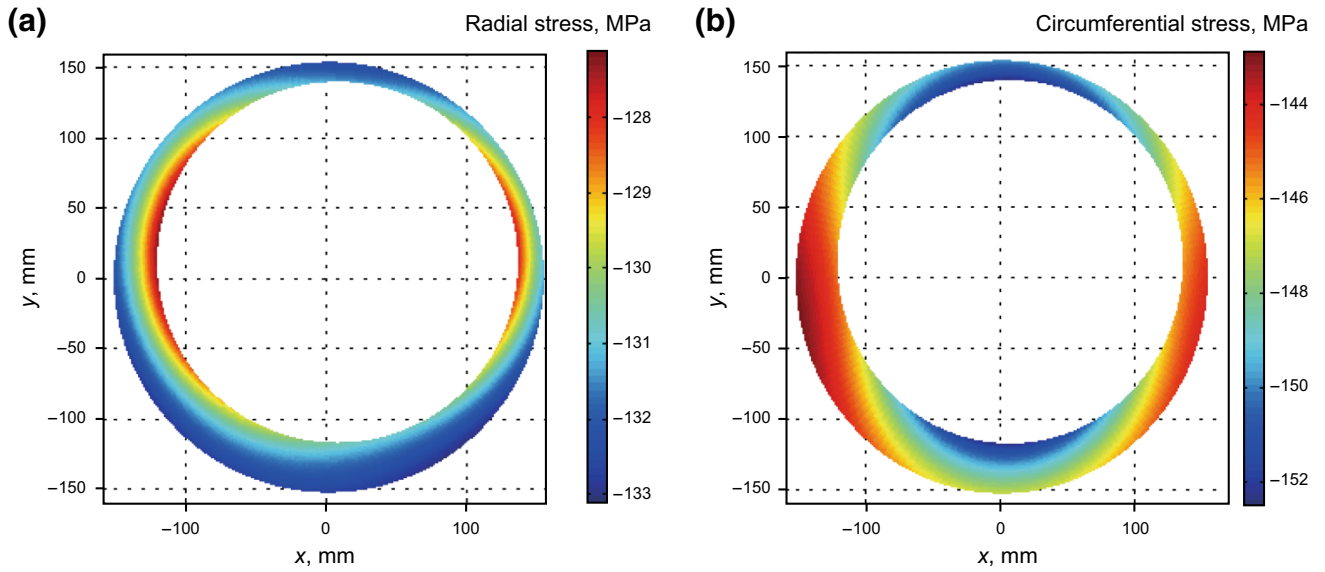


**Fig. 11** Stress distribution in the cement sheath. **a** Radial stress. **b** Circumferential stress

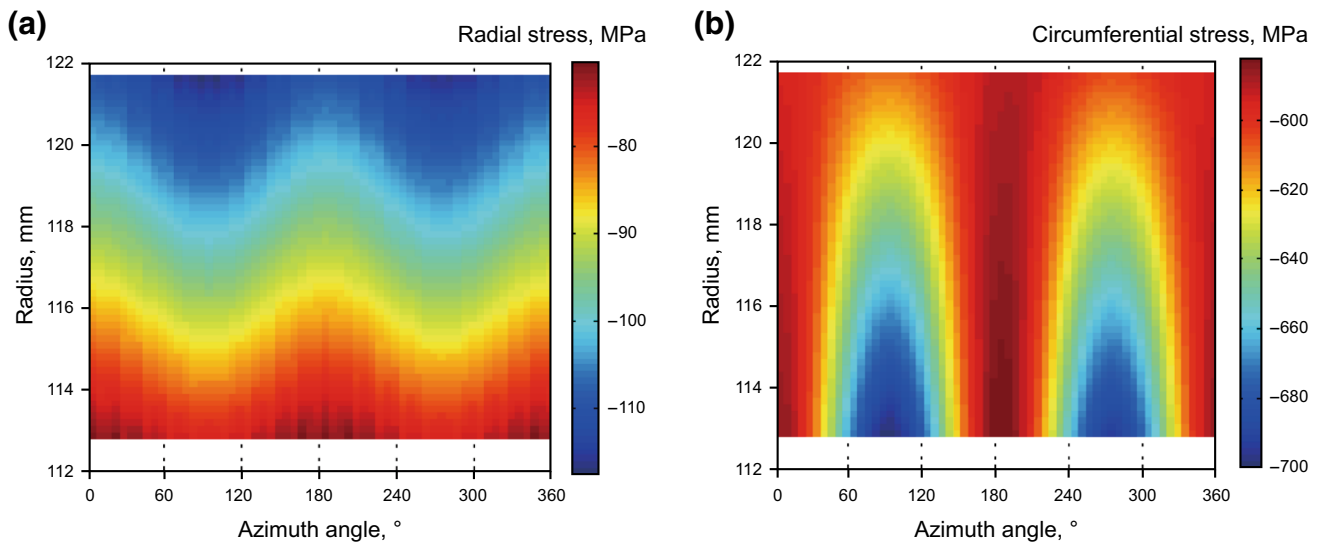


**Fig. 12** Stress distribution in the casing. **a** Radial stress. **b** Circumferential stress

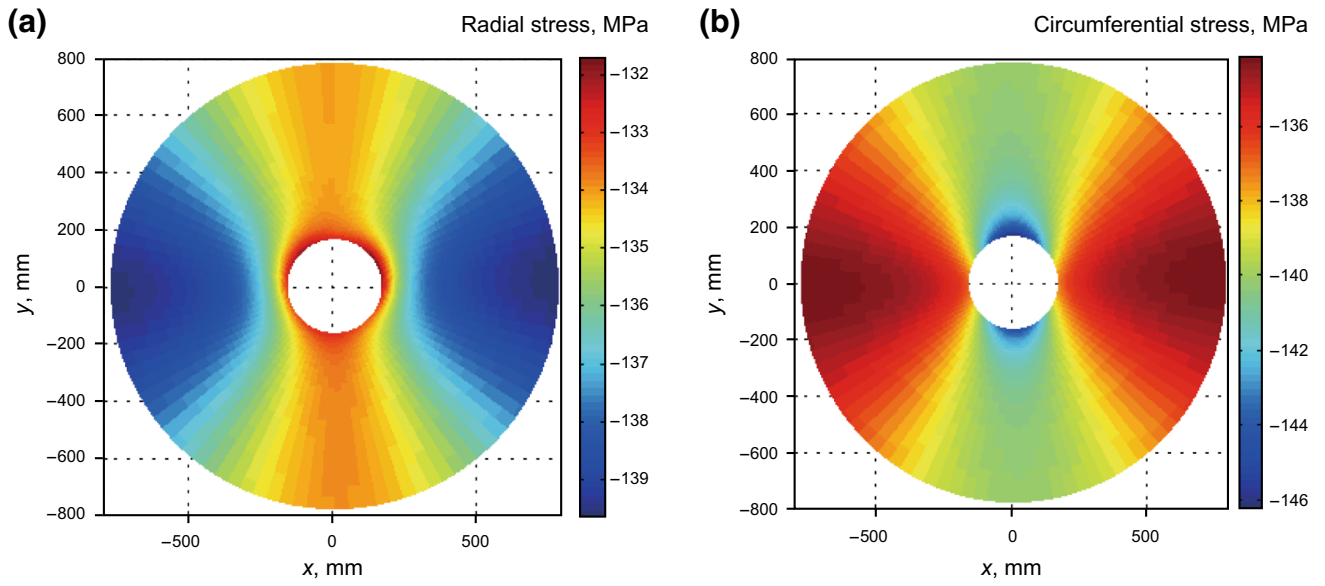


Fig. 13 Stress in the salt formation. a Radial stress. b Circumferential stress

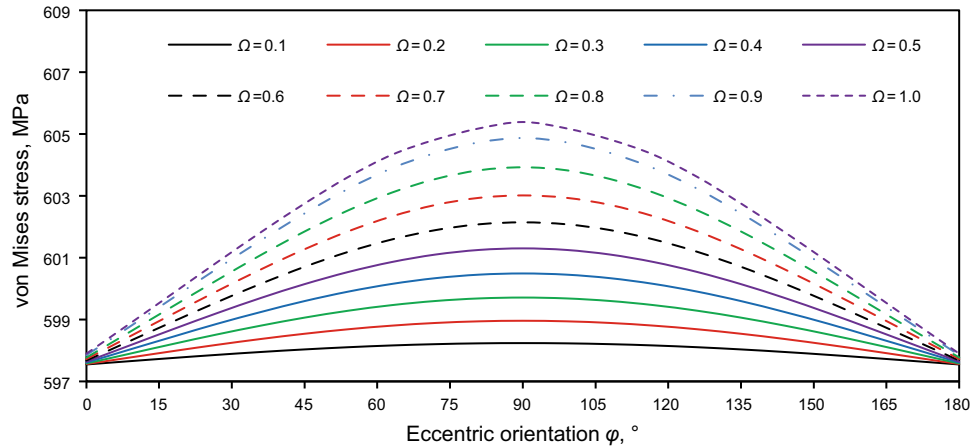
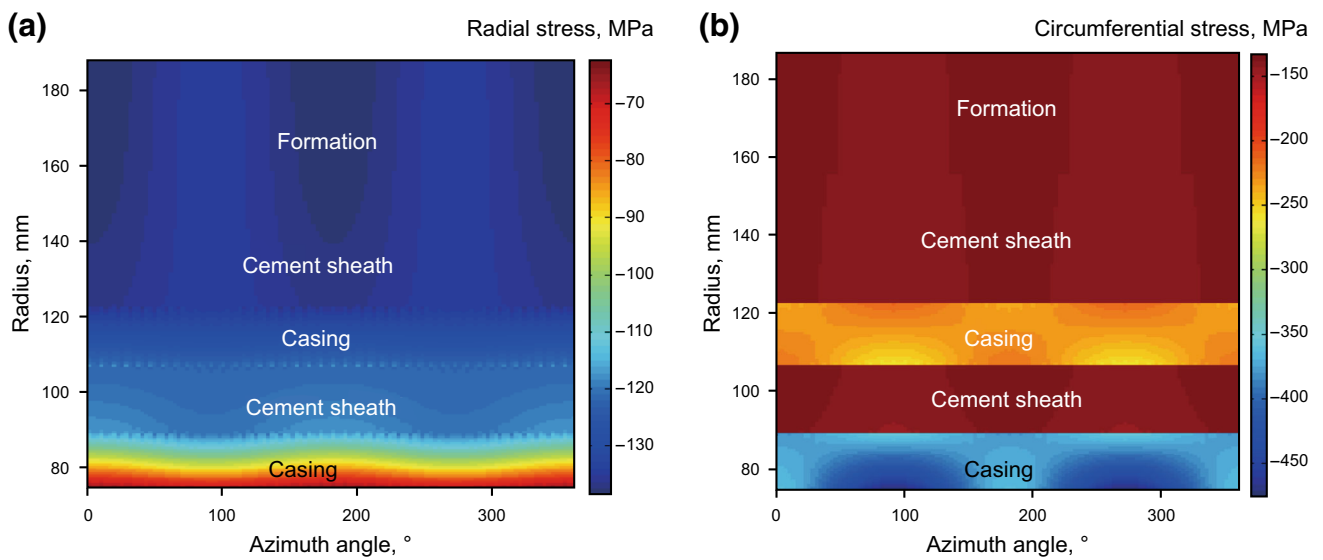


Fig. 14 Eccentricity versus the maximum von Mises stress in the casing

Table 4 Related parameters of multi-casing in the wellbore

$E_1, E_2, E_3, E_4, E_5$ , GPa	$\nu_1, \nu_2, \nu_3, \nu_4, \nu_5$	$r_1, r_2, r_3, r_4, r_5$ , mm	$S_H, S_h$ , MPa	$P_0$ , MPa
210, 7, 210, 7, 5	0.30, 0.18, 0.30, 0.18, 0.45	73, 88.9, 106.3, 122.2, 155.6	-140, -134	61.25



**Fig. 15** Stresses in the multi-casing structure (180 boundary elements in total). **a** Radial stress. **b** Circumferential stress

**Table 5** Related parameters of the wellbore in the Tarim Basin

$E_1, E_2, E_3$ , GPa	$\nu_1, \nu_2, \nu_3$	$r_1, r_2, r_3$ , mm	$S_H, S_h$ , MPa	$P_0$ , MPa	Eccentricity
210, 7, 5	0.30, 0.18, 0.45	109.5, 125.4, 155.6	-20, -10	5	[0, 0°]

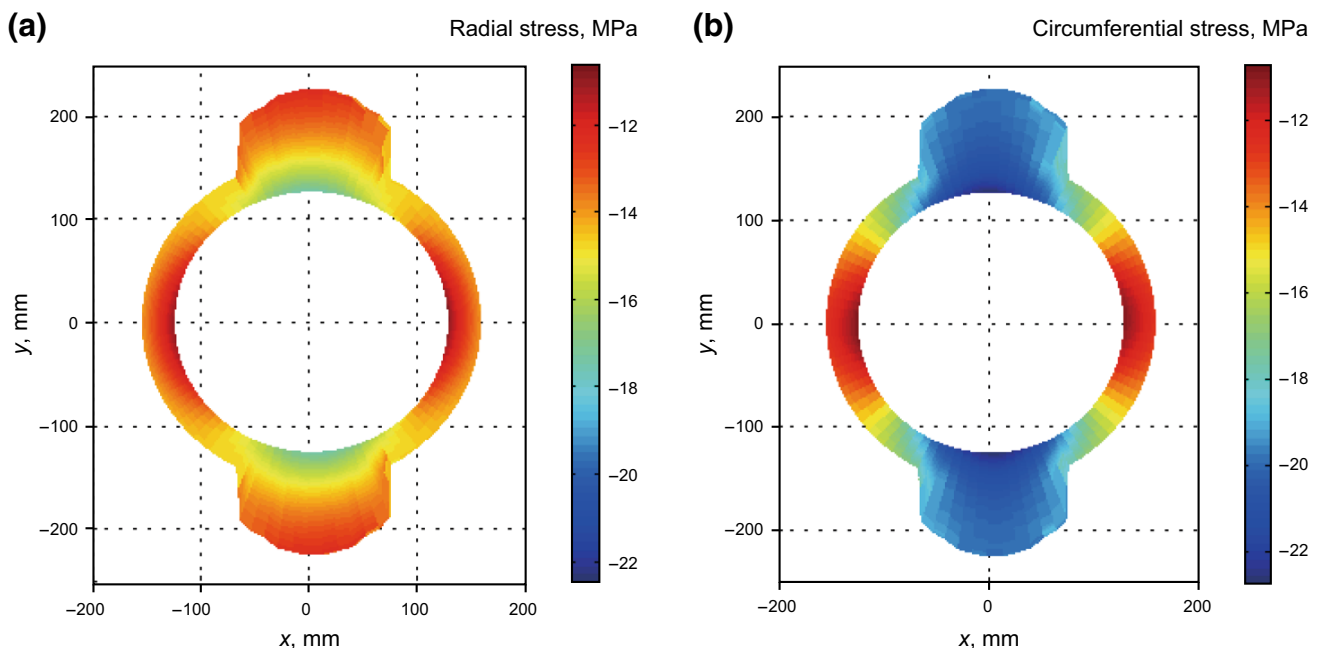


**Fig. 16** Stresses in the cement sheath. **a** Radial stress. **b** Circumferential stress

along the radius while the circumferential stress is not continuous at the interface. The radial stress decreases and the circumferential stress increases with increasing interfacial gap between the adjacent materials.

**Acknowledgements** This research was supported by the China National High Technology Research and Development Program 863 (Grant No. 2013AA064503). The China Scholarship Council is thanked for supporting the first author of this paper to visit the Georgia Institute of Technology, USA.

**Open Access** This article is distributed under the terms of the Creative Commons Attribution 4.0 International License (<http://creativecommons.org/licenses/by/4.0/>), which permits unrestricted use, distribution, and reproduction in any medium, provided you give appropriate credit to the original author(s) and the source, provide a link to the Creative Commons license, and indicate if changes were made.

## References

- Bobet A. Lined circular tunnels in elastic transversely anisotropic rock at depth. *Rock Mech Rock Eng.* 2011;44:149–67. doi:10.1007/s00603-010-0118-1.
- Cheng W, Jin Y, Li H, Chen M. A novel linear triangular element of three-dimensional displacement discontinuity method. *Eng Anal Bound Elem.* 2015;59:89–96. doi:10.1016/j.enganabound.2015.04.020.
- Crouch SL. Solution of plane elasticity problems by the displacement discontinuity method. *Int J Numer Methods Eng.* 1976;10:301–43. doi:10.1002/nme.1620100206.
- Crouch SL, Starfield AM. *Boundary element methods in solid mechanics.* London: Goerge Allen and Unwin Publishers; 1983.
- Elleithy WM, Tanaka M. Interface relaxation algorithms for BEM–BEM coupling and FEM–BEM coupling. *Comput Methods Appl Mech Eng.* 2003;192(26):2977–92. doi:10.1016/S0045-7825(03)00312-8.
- Gun H, Gao XW. Analysis of frictional contact problems for functionally graded materials using BEM. *Eng Anal Bound Elem.* 2014;38:1–7. doi:10.1016/j.enganabound.2013.10.004.
- Ghassemi A, Cheng AHD, Diek A, et al. A complete plane strain fictitious stress boundary element method for poroelastic media. *Eng Anal Bound Elem.* 2001;25:25–41. doi:10.1016/S0955-7997(00)00046-1.
- Ghassemi A, Zhang Q. A transient fictitious stress boundary element method for porothermoelastic media. *Eng Anal Bound Elem.* 2004;28:1363–73. doi:10.1016/j.enganabound.2004.05.003.
- Kandilas CB. Transient elastodynamic analysis of nonhomogeneous anisotropic plane bodies. *Acta Mech.* 2012;223:861–78. doi:10.1007/s00707-011-0607-7.
- Luo JF, Liu YJ, Berger EJ. Interfacial stress analysis for multi-coating systems using an advanced boundary element method. *Comput Mech.* 2000;24:448–55. doi:10.1007/s004660050004.
- Mastin L. Effect of borehole deviation on breakout orientations. *J Geophys Res.* 1988;93(B8):9187–95.
- Park KH. A BEM formulation for inhomogeneous potential problems by particular integrals. *Appl Math Model.* 2003;27:293–306. doi:10.1016/S0307-904X(02)00125-7.
- Ritz E, Mutlu O, Pollard DD. Integrating complementarity into the 2D displacement discontinuity boundary element to model faults and fractures with frictional contact properties. *Comput Geosci.* 2012;45:304–12. doi:10.1016/j.cageo.2011.11.017.
- Soares JD, von Estorff O, Mansur WJ. Iterative coupling of BEM and FEM for nonlinear dynamic analyses. *Comput Mech.* 2004;34(1):67–73. doi:10.1007/s00466-004-0554-4.
- Sladek V, Sladek J, Markechova I, et al. An advanced boundary element method for elasticity problems in nonhomogeneous media. *Acta Mech.* 1993;97:71–90. doi:10.1007/BF01173143.
- Wang H, Towler BF, Soliman MY. Near wellbore stress analysis and wellbore strengthening for drilling depleted formations. In: *Rocky mountain oil & gas technology symposium*, 16–18 April, Denver, Colorado, USA. 2007. doi:10.2118/102719-MS.
- Zhang F, Zhang S, Jiang X, et al. Borehole stability in naturally fractured reservoirs during production tests. *Pet Sci.* 2008;5:247–50. doi:10.1007/s12182-008-0039-8.
- Zheng R, Coleman CJ, Thien NP. A boundary element approach for non-homogeneous potential problems. *Comput Mech.* 1991;7:279–88. doi:10.1007/BF00370041.
- Zoback MD, Barton CA, Brudy M, Castillo DA, et al. Determination of stress orientation and magnitude in deep wells. *Int J Rock Mech Min Sci.* 2003;40(7):1049–76. doi:10.1016/j.ijrmms.2003.07.001.